Trends in Chemistry

CellPress REVIEWS

Opinion

Synthetic Engineering of Graphene Nanoribbons with Excellent Liquid-Phase Processability

Wenhui Niu,[1,2,4] Junzhi Liu,[2,4] Yiyong Mai,[1,*] Klaus Müllen,[3] and Xinliang Feng[2,*]

Over the past decade, the bottom-up synthesis of structurally defined graphene nanoribbons (GNRs) with various topologies has attracted significant attention due to the extraordinary optical, electronic, and magnetic properties of GNRs, rendering them suitable for a wide range of potential applications (e.g., nanoelectronics, spintronics, photodetectors, and hydrothermal conversion). Remarkable achievements have been made in GNR synthesis with tunable widths, edge structures, and tailor-made functional substitutions. In particular, GNRs with liquid-phase dispersibility have been achieved through the decoration of various functional substituents at the edges, providing opportunities for revealing unknown GNR physiochemical properties. Because of the promise of liquid-phase dispersible GNRs, this mini-review highlights recent advances in their synthetic strategies, physiochemical properties, and potential applications. In particular, deep insights into the advantages and challenges of their syntheses and chemical methodologies are provided to encourage future endeavors and developments.

Highlights

Structurally well-defined graphene nanoribbons (GNRs) with excellent liquid-phase processability have been achieved through the introduction of functional substituents on the edge periphery of GNRs.

Physicochemical properties of GNRs in the liquid phase have been disclosed, such as select photophysical properties and supramolecular behavior.

GNRs with excellent solution processability show great potential in applications, including field effect transistors (FETs), chemical sensors, and photothermal conversion, among others.

Bottom-up Synthesis of Structurally Defined Graphene Nanoribbons

Graphene nanoribbons (GNRs), defined as nanometer-wide strips of graphene, have attracted significant attention as candidates for next-generation semiconductor materials [1–6]. Quantum confinement effects provide GNRs with semiconducting properties, namely, with a finite bandgap that critically depends on their width and edge structures [7–10]. In the past decade, significant effort has been devoted to the synthesis of high-quality GNRs with narrow widths and smooth edges [9,11,12]. Two main strategies have been established for the synthesis of GNRs thus far: 'top-down' and 'bottom-up' approaches. The top-down approach includes the lithographic etching of graphene and unzipping of carbon nanotubes [13–17]. However, these methods generally suffer from low yields and poor structural precision, leading to GNRs with uncontrollable widths and edge structures. Moreover, to achieve precise bandgap control, GNRs should be narrower than 5 nm, which is at the precision limit for the start-of-the-art top-down techniques. In contrast, bottom-up strategies based on the 'on-surface synthesis' or 'solution-based chemical synthesis', namely, 'graphitization' and 'planarization' of tailor-made three-dimensional (3D) polyphenylene precursors, allows access to structurally well-defined GNRs with tunable widths as well as atomically precise edges, including armchair, zigzag, and cove structures [18–22]. Moreover, the precise positioning of heteroatom dopants in GNRs can be realized via this strategy, opening up another pathway for tailoring their optical and electronic properties [23–26].

The liquid-phase processability of GNRs is essential for investigating their fundamental physiochemical properties in solution and for the fabrication of nanoelectronic devices via dip coating or drop casting GNR dispersions on solid substrates [1,27–39]. Compared with the surface-

[1]School of Chemistry and Chemical Engineering, Shanghai Key Laboratory of Electrical Insulation and Thermal Ageing, Shanghai Jiao Tong University, 200240 Shanghai, China
[2]Center for Advancing Electronics Dresden (cfaed), Faculty of Chemistry and Food Chemistry, Technische Universität Dresden, 01062 Dresden, Germany
[3]Max Planck Institute for Polymer Research, Ackermannweg 10, 55128 Mainz, Germany
[4]These authors contributed equally to this work.

*Correspondence:
mai@sjtu.edu.cn (Y. Mai),
xinliang.feng@tu-dresden.de (X. Feng).

assisted method, solution-synthesis approaches show significant advantages for the large-scale preparation of liquid-phase-dispersible GNRs [40–43]. Substantial efforts have recently been devoted to the solution-phase synthesis of GNRs and several elegant protocols have been developed. Several types of all-carbon or heteroatom-doped GNRs with excellent liquid-phase processability have been synthesized [11,12,24–26,43–52]. In this opinion article, we focus our discussion on our recent contributions in this emerging research area. Following a general introduction, the second section presents synthetic strategies for accessing different types of liquid-phase-dispersible GNRs. The third part concentrates on the supramolecular nanostructures derived from polymer-functionalized GNRs by taking advantage of their enhanced dispersibility and amphiphilicity in the liquid phase. The fourth section describes several typical applications of GNRs profiting from their excellent liquid-phase processability, including field effect transistors (FETs), chemical sensors, and photothermal conversion. The final section presents a summary and outlook of the field.

Synthetic Strategies toward Liquid-Phase-Processable GNRs

GNRs can easily aggregate in the solid state and in solution due to the strong π–π interactions between their large conjugated sp^2-carbon planes. Both physical approaches (i.e., sonication exfoliation [26] and chemical treatment with a strong acid [53]) have been tested for enhancing the liquid-phase GNR dispersion. However, these approaches generally have limited dispersion effects and visible agglomerates remain. To overcome the strong π–π interactions between the GNR backbones while keeping their aromatic backbone intact, the introduction of functional substituents on the periphery of the GNRs has proven to be a feasible strategy. To date, three primary approaches have been established for achieving liquid-phase-dispersible GNRs. The first method relies on the introduction of alkyl substituents (Figure 1A–C). For instance, dodecyl-decorated arm-chair-edged GNRs (**GNR 1**) with a lateral width of 0.7–1.1 nm and lengths of over 200 nm have been synthesized by the Diels-Alder reaction of AB-type monomer **1** (Figure 1A) [41], in which the dodecyl chains were installed in the initial stage of the synthesis (monomer **1**), affording GNRs with good liquid-phase dispersibility. Upon strong sonication, **GNR 1** could be dispersed in common organic solvents [e.g., tetrahydrofuran (THF), chlorobenzene, trichlorobenzene (TCB) and *N*-methylpyrrolidone (NMP)] with typical concentrations of up to ~0.01 mg/ml (calculated for the GNR backbone unless otherwise specified). Compared with linear alkyl chains, decoration with branched side chains could further improve the dispersibility [54]. For instance, branched 2-decyltetradecyl chains have been grafted at the edge of GNRs with the same backbone as **GNR 1** (**GNR 2**, Figure 1A). These branched alkyl chains are sterically bulkier than the linear dodecyl chains and are thus better able to disrupt the intermolecular π–π interactions of the GNRs. As a consequence, the concentration of **GNR 2** in THF reaches 0.2 mg/ml, which is more than one order of magnitude higher than that of **GNR 1**. The UV-Vis absorption spectrum of a dispersion of **GNR 1** in NMP reveals an absorption maximum at 550 nm and an optical bandgap of 1.88 eV (Figure 1E). A scanning probe microscopy investigation of **GNR 1** on highly oriented pyrolytic graphite (HOPG) demonstrated that straight GNRs coaligned into domains with unique noodle-like structures (Figure 1F), while **GNR 2** self-assembled into ordered monolayers with longitudinal lengths of over 200 nm (Figure 1G).

By tailoring the position of the peripheral alkyl chains, **GNRs 3** and **4**, both with widths of 1.5 nm and lengths of ca. 100 nm, were also synthesized by a Diels-Alder approach from monomers **2** and **3**, respectively (Figure 1B) [49]. **GNR 3** possesses a planar geometry, while **GNR 4** adopts a nonplanar conformation due to the steric repulsion between the aromatic protons and the introduced alkyl chains (Figure 1B). The different backbone geometries result in **GNRs 3** and **4** having distinct dispersibilities in organic solvents; **GNR 4** shows superior solution dispersibility in THF and TCB. Based on theoretical calculations and experimental characterization, the optical bandgaps of **GNR 3** and **4** were estimated to be 1.45 and 1.18 eV, respectively (Figure 1D).

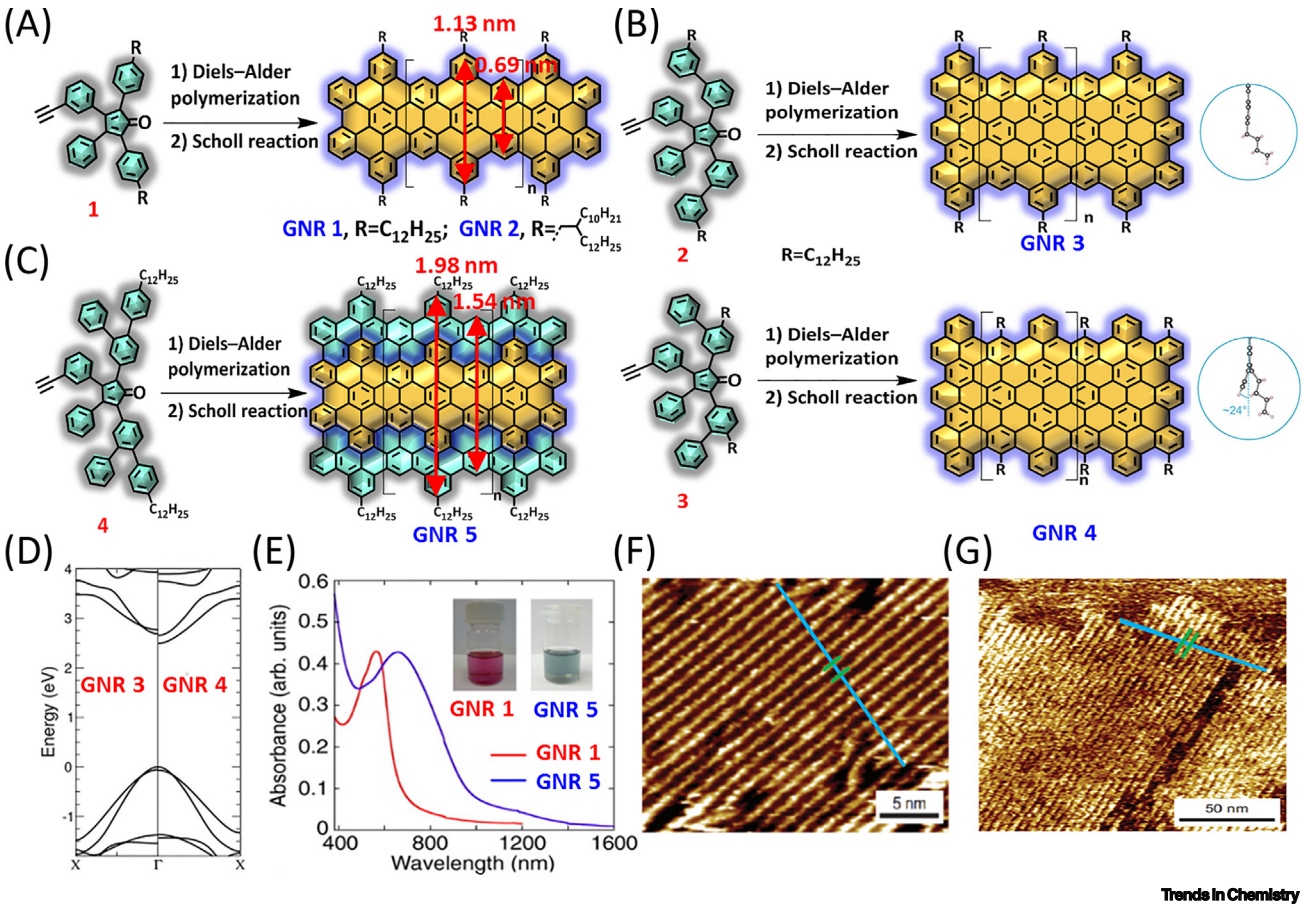

Figure 1. Synthesis and Characterization of Alkyl Chain Functionalized Graphene Nanoribbons (GNRs). (A) Schematic of **GNR 1** functionalized with linear alkyl chains and **GNR 2** decorated with branched alkyl chains. (B) Chemical structures of **GNRs 3** and **4**. Insets: zoomed-in images of the side views of **GNRs 3** and **4** in the edge region reveal distinct structural distortions. (C) Illustration of **GNR 5**. (D) Band structures of **GNRs 3** and **4** calculated by the GW method. (E) Normalized UV-Vis-near-infrared absorptions of **GNR 1** and **5** in tetrahydrofuran (THF). Inset: photos of the THF dispersions of **GNRs 1** and **5**. (F,G) Scanning probe microscopy images of **GNR 1** and **GNR 2**, respectively, on highly oriented pyrolytic graphite. Adapted, with permission, from [34,41,49].

These results suggest that the optoelectronic properties of GNRs can be modulated by adjusting both their width and planarity.

To expand the width of the GNRs, laterally extended arm-chair-edged **GNR 5** was synthesized by the Diels-Alder reaction of monomer **4** substituted with linear dodecyl chains, and a width of ca. 2 nm and a length over 100 nm were obtained (Figure 1C) [34]. Compared with **GNR 1**, **GNR 5** exhibits a smaller optical bandgap of ~1.2 eV and a broader optical absorption extending to the near infrared (NIR) region (Figure 1E). In addition, **GNR 5** shows dispersibility in common organic solvents (e.g., THF and TCB) with typical concentrations of approximately 0.06 mg/ml.

The second powerful strategy to promote the dispersibility of GNRs is functionalization with polymer chains. The dimensions of polymer chains with high molecular weights are much larger than those of alkyl chains. Therefore, the substitution of polymer chains on the periphery of GNRs may be more effective for disrupting the intermolecular π–π interactions, affording GNRs with significantly enhanced liquid-phase processability. In this respect, structurally defined GNRs with a width of 1.7 nm and lengths of 15–60 nm were synthesized from monomer **3** by the Yamamoto polymerization approach, and flexible poly(ethylene oxide) (PEO) chains were

then grafted onto the ribbons (Figure 2A, **GNR-PEO**) [55]. The resultant **GNR-PEO** exhibited superior dispersibility in conventional organic solvents with a concentration of ~1 mg/ml. Impressively, **GNR-PEO** was even dispersible in an aqueous phase with a concentration of ~0.2 mg/ml. The UV-Vis spectrum of **GNR-PEO** in THF shows a maximum absorption at ~650 nm and the corresponding optical bandgap is estimated to be ~1.3 eV (Figure 2B). In contrast, a significantly redshifted absorption was observed for **GNR-PEO** in H_2O, which is attributed to the aggregation of the GNRs induced by hydrophobic and π–π interactions. The fluorescence of GNRs is generally quenched in solution due to their substantial aggregation; hence, the characterization of their photoluminescence (PL) is generally difficult. Notably, the excellent dispersibility of **GNR-PEO** enables the acquisition of their PL spectra, which exhibit an emission maximum at ~920 nm in the NIR region (in THF), while the PL is completely quenched in water due to strong aggregation.

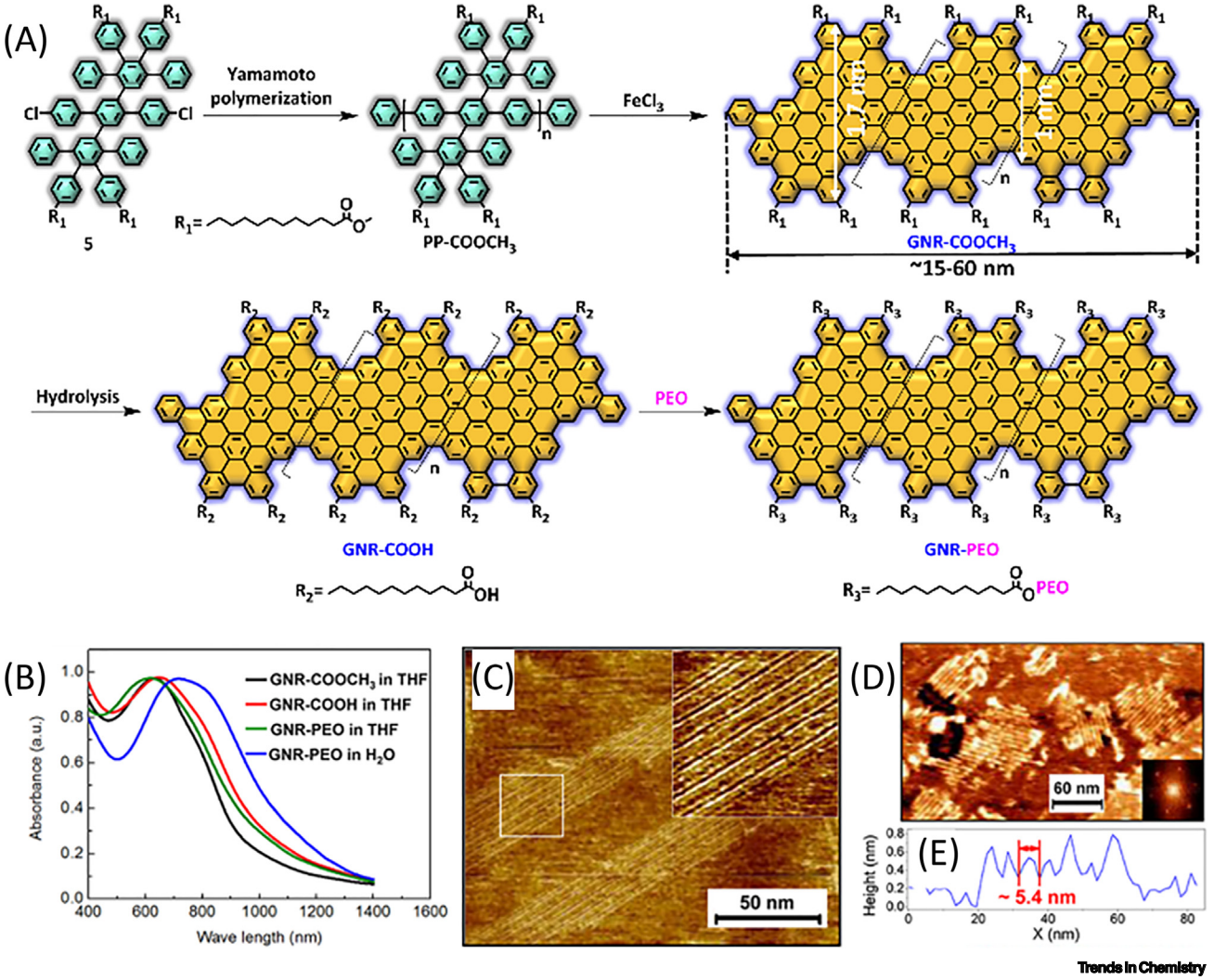

Figure 2. Synthesis and Characterization of Poly (Ethylene Oxide) Functionalized Graphene Nanoribbons (**GNR-PEO**). (A) Illustration of the synthetic route toward **GNR-PEO**. (B) UV-Vis-near infrared spectra of the GNRs. (C,D) Scanning probe microscopy (SPM) images of **GNR-PEO** at the trichlorobenzene (TCB)/highly oriented pyrolytic graphite interface. (E) The line profile along the black broken line in the SPM image in panel (D) shows the formation of a monolayer film. Adapted, with permission, from [55]. Abbreviation: THF, Tetrahydrofuran.

The third strategy involves the introduction of bulky 3D substituents at the periphery of the GNRs, the dimension of which are larger than the interlayer distance (~0.34 nm) of graphite. By this means, bulky groups can significantly disrupt the π–π stacking of the GNRs and facilitate the dispersion of single ribbons in the liquid phase. Very recently, a novel type of structurally defined arm-chair GNR was synthesized from monomer **6** by the Yamamoto polymerization protocol (Figure 3A, **GNR-AHM**). The monomers were decorated with pendant Diels-Alder cycloadducts of anthracenyl units and *N*-*n*-hexadecyl maleimide (AHM), which have a 3D dimension of 0.5 nm [56]. As a result, three GNRs with widths of 1.7 nm and different lengths (6, 11, and 58 nm) were synthesized (denoted **GNR-AHM-1**, **2**, and **3** in Figure 3). The **GNR-AHMs** exhibited unprecedented liquid-phase dispersibility. Specifically, homogeneous dispersions could be readily generated by a mild shake or sonication of **GNR-AHM** in common organic solvents, including THF, dichloromethane, toluene, and TCB, with a record-high concentration of 5 mg/ml. Compared with that of **GNR-PEO**, the UV-Vis spectra of **GNR-AHMs** in THF show obviously blue-shifted narrow absorptions along with the appearance of distinct fingerprint signals (Figure 3B), suggesting that **GNR-AHMs** are less prone to aggregation. PL spectroscopy analysis revealed that dilute dispersions of **GNR-AHMs** in THF (<0.1 mg/ml) consist mainly of nonaggregated ribbons, exhibiting NIR emissions with high quantum yield (9.1%) and long lifetime (8.7 ns) (Figure 3C). Moreover, the outstanding solution processability allows the real-time ultrafast excited-state dynamics of the GNRs to be resolved, and these ribbons display features of isolated molecules in solution, confirming the dispersion of the single ribbons in organic solvents.

Supramolecular Nanostructures of PEO-Functionalized GNRs

The supramolecular behavior of nanographenes has been widely explored in the past decades, including their self-assembly in solution [57,58] and bulk liquid-crystalline phase formation

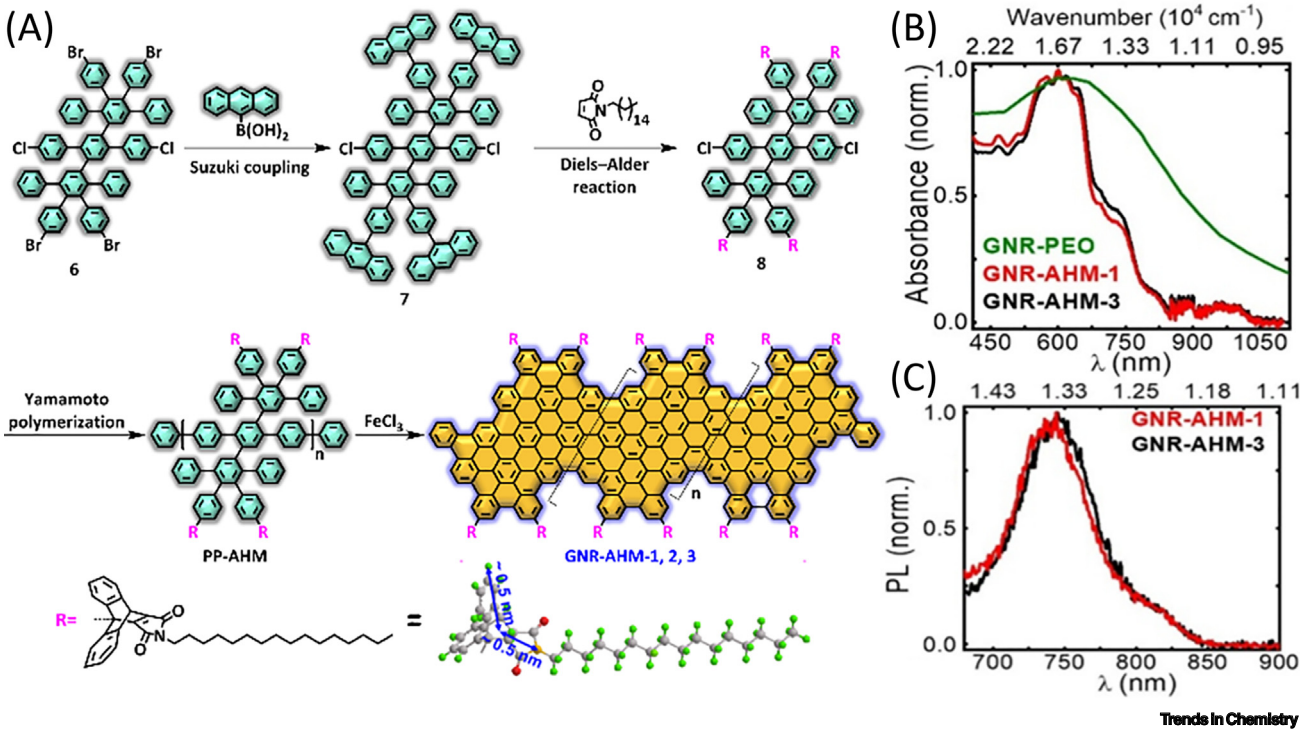

Figure 3. Synthesis and Characterization of *N*-*n*-Hexadecyl Maleimide Functionalized Graphene Nanoribbons (**GNR-AHM**). (A) Illustration of the synthetic route toward **GNR-AHM**. (B) Absorption and (C) photoluminescence (PL) spectra of **GNR-AHMs** in tetrahydrofuran. Adapted, with permission, from [56].

[59–61]. For instance, Aida and colleagues reported the self-assembly of amphiphilic hexa-*peri*-hexabenzocoronenes (HBCs) decorated with acceptor trinitrofluorenone groups into nanotubes and microfibers, which showed a photoconductive response with a large on/off ratio [57,58]. Müllen and colleagues reported that alkyl chain-substituted HBCs formed a discotic liquid-crystalline phase associated with high charge-carrier mobility [59–61]. In comparison with smaller HBCs, the supramolecular behavior of GNRs in the liquid phase is less frequently investigated, mainly due to their poor liquid-phase dispersibility [53,62,63]. Although alkyl chain-functionalized GNRs can self-organize into monolayers at the solid–liquid interface (Figure 1F), their poor dispersibility in organic solvents limits the diversity of GNR supramolecular nanostructures. In contrast, polymer functionalization provides GNRs with enhanced dispersibility and amphiphilicity, enabling the supramolecular self-assembly of the resultant GNRs both at the solid–liquid interface and in solution [30,55]. For example, **GNR-PEOs** with different PEO lengths show controllable supramolecular behavior (see Figure 4 for the self-assembly of **GNR-PEO400**, **GNR-PEO1000**, and **GNR-PEO2000**; the numbers represent the molecular weights of the PEO chains). At the liquid–solid (e.g., TCB–HOPG) interface, **GNR-PEO** forms raft-like self-assembled monolayers with longitudinal sizes of >100 nm, in which individual GNRs were coaligned by a combination of side-by-side and end-to-end alignment (Figure 2C–E) [55]. In the aqueous phase, the length of the PEO chains determines the hydrophilic-to-hydrophobic ratio of **GNR-PEO** and thus significantly affects the morphology of their aggregates. As a result, **GNR-PEOs** could self-organize into 1D hierarchical supramolecular nanostructures, including ultralong

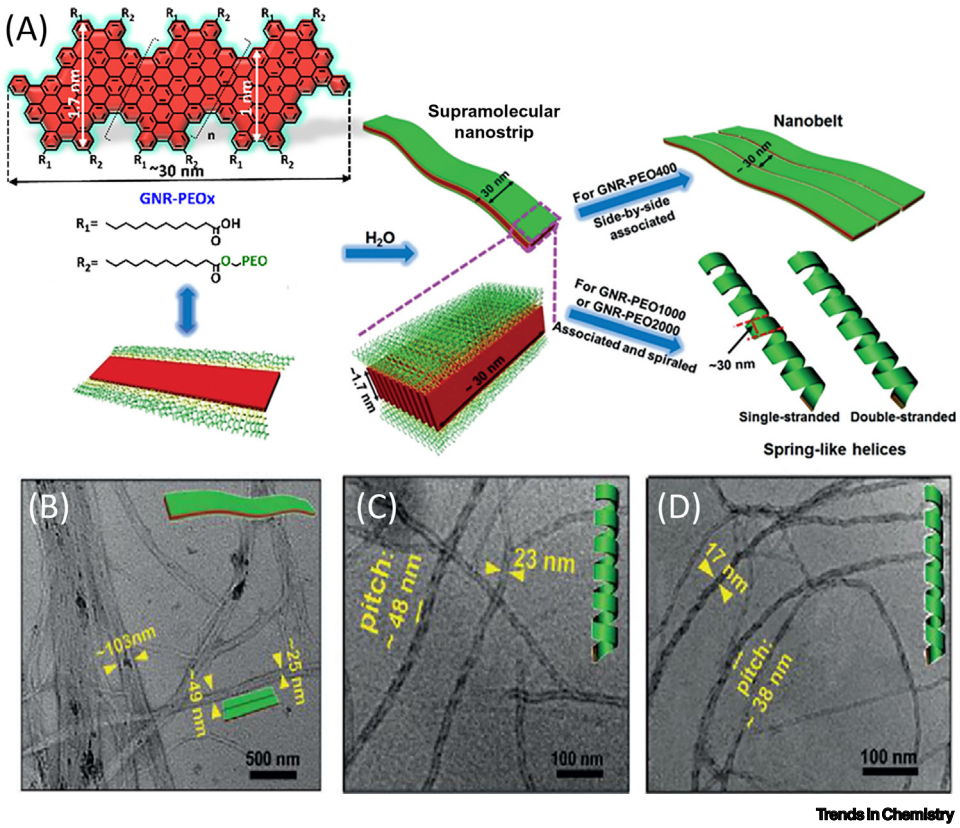

Figure 4. Illustration of Supramolecular Behavior and Morphology of Poly (ethylene oxide) Functionalized Graphene Nanoribbons (**GNR-PEO**). (A) Illustration of the molecular structure of **GNR-PEOx** and its possible hierarchical self-assembly mechanism in H_2O. (B–D) Typical transmission electron microscopy images of the superstructures formed by **GNR-PEO400** (B), **GNR-PEO1000** (C), and **GNR-PEO2000** (D) in water. Adapted, with permission, from [30].

nanobelts and nanohelices (Figure 4), depending on the PEO chain lengths [29]. A mechanistic study revealed that **GNR-PEO400**, with the shortest PEO side chains, first aggregated into small nanostrips and then the belt-like superstructures associated with each other by a side-by-side alignment due to the small interchain steric hindrance among the side PEO coils (Figure 4B). In contrast, the longer PEO coils around the nanostrips formed by **GNR-PEO1000** or **GNR-PEO2000** are more crowded, generating large interchain steric hindrance and resulting in high system energy. To relieve the high energy, spring-like helices were formed, providing more peripheral space for the accommodation of the PEO side chains (Figure 4C,D).

Potential Applications

After achieving excellent solution processability, a number of potential applications for GNRs processed from the liquid phase have been developed [27,30,38,55,62–65]. As one of the typical examples, GNR-film-based chemical sensors have been fabricated using **GNR 1** with lengths of >500 nm and widths of ~0.78 nm. To image and characterize the GNRs, dodecyltriethoxysilane functionalized Si/SiO_2 substrates and a high-boiling solvent, 1-cyclohexyl-2-pyrrolidone (CHP), were required. The resultant GNR-based sensors demonstrated exceptional NO_2-sensing performance with high sensitivity for NO_2 concentrations down to parts per billion levels [27]. The second application refers to GNR-based FETs. With the advantage of dispersibility in common organic solvents, **GNR-PEO** films with micrometer-scale lateral dimensions were fabricated at the liquid–solid interface using a high concentration of GNRs (0.5 mg/ml) [55]. GNR thin-film-based FETs ($3 \times 3\ \mu m^2$) were constructed between Ti/Au electrodes on Si/SiO_2 substrates (Figure 5). The substrates were heated to evaporate the solvent and then annealed at 500°C to cleave the insulating PEO chains to reduce ribbon-to-ribbon junction resistance and improve the conductivity of the GNR device. The resultant

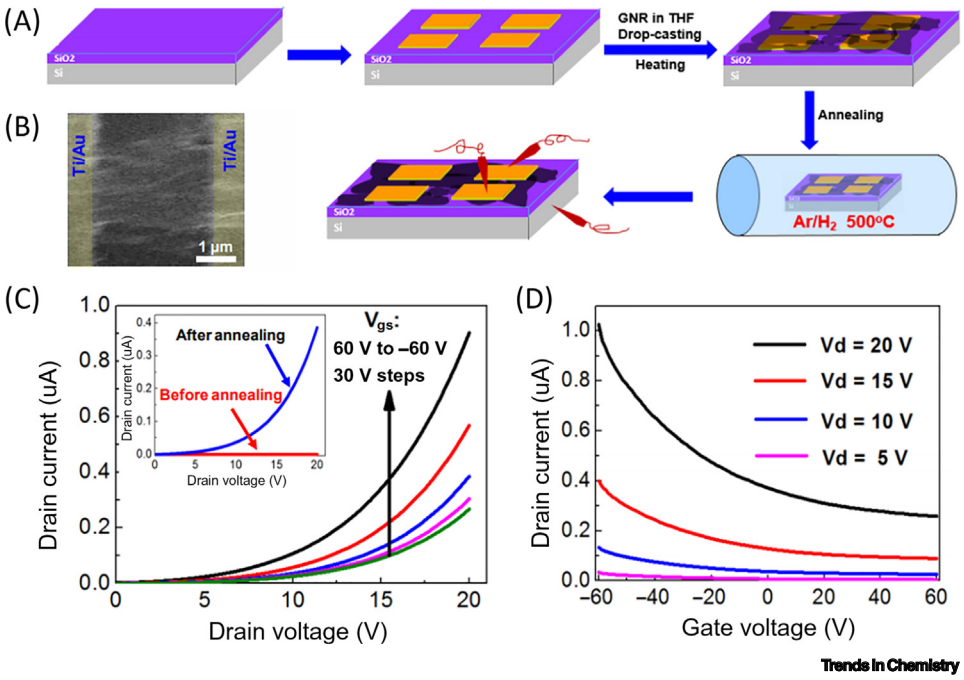

Figure 5. Field Effect Transistor (FET) Fabrication and Characterization. (A) Schematic of the fabrication of a graphene nanoribbon-poly(ethylene oxide) (**GNR-PEO**) thin-film-based FET. (B) Scanning electron microscopy image of the thin film between two Ti/Au electrodes (2 nm-Ti/30 nm-Au prepared by E-beam lithography and E-beam evaporation). (C) Current versus drain voltage (I–Vd) of the FET under different gate voltages (V_{gs}). Inset: I–Vd of the FET before (red) and after (blue) annealing at 500°C (V_{gs} = 0 V). (D) I–V_{gs} of the FET under different drain voltages. Adapted, with permission, from [55]. Abbreviation: THF, Tetrahydrofuran.

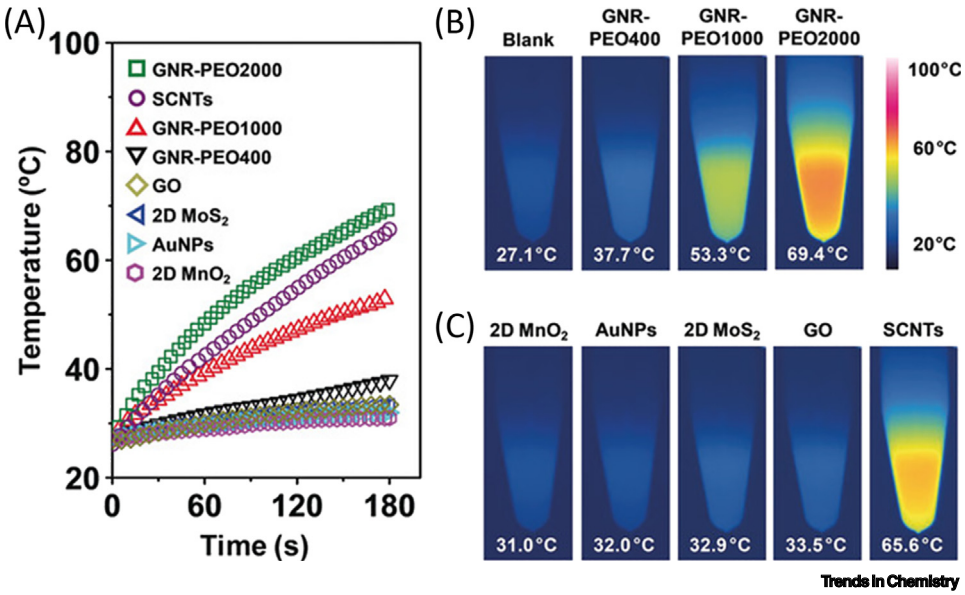

Figure 6. Photothermal Conversion Characterization. (A) The time-dependent temperature increase of aqueous dispersions of Poly (ethylene oxide) functionalized Graphene Nanoribbons GNR-PEO and other low-dimensional materials under near infrared irradiation (808 nm, 2.5 Wcm^{-2}). (B) Thermal images of the GNR-PEO aqueous dispersions. (C) Thermal images of the aqueous dispersions of different low-dimensional materials. Adapted, with permission, from [30]. Abbreviations: AuNPs, gold nanoparticles; GO, graphene oxide; MnO_2, manganese dioxide; MoS_2, molybdenum disulfide; SCNTs, single-walled carbon nanotubes.

thin-film FETs exhibited a maximum carrier mobility of ~0.3 $cm^2 V^{-1} s^{-1}$ under a low voltage (20 V), highlighting the applicability of **GNR-PEO** in FETs [55]. As the third representative application, the photothermal conversion of GNR superstructures has recently been demonstrated in the aqueous phase [30]. With NIR absorption and excellent water dispersibility, the **GNR-PEO** superstructures in water exhibited high photothermal conversion with an efficiency of 31%, superior to those of many conventional low-dimensional nanomaterials, such as single-walled carbon nanotubes, graphene oxide, gold nanoparticles, 2D molybdenum disulfide, and 2D manganese dioxide (Figure 6) [30]. The excellent photothermal conversion performance affords great opportunities for the application of GNRs in photothermal tumor therapy, antisepsis, and other applications.

Concluding Remarks

Bottom-up chemical synthesis techniques allow the precise control of GNR structures and their functionalization at the molecular level. Thus far, decoration by alkyl chains, polymer coils, and bulky side groups at the edges of GNRs have been demonstrated, and these substituents afforded GNRs with excellent liquid-phase dispersibility. The successful bottom-up synthesis of atomically precise GNRs with excellent solution processability opens tremendous opportunities, not only for revealing the intrinsic electronic properties of individual ribbons but also for exploring the potential applications of GNRs in numerous fields, including nanoelectronics, spintronics, gas sensors, and photothermal conversion.

Despite the remarkable progress made in the past decade, several challenges remain to be addressed in the ongoing development of liquid-phase dispersible GNRs (see Outstanding Questions). Included in these challenges are as follows.

(i) That the topological structure of GNRs is mostly limited to arm-chair edged ribbons. All zigzag edge configurations and combined edge structures (e.g., arm-chair, cove, and zigzag)

Outstanding Questions

The topologies of GNRs are thus far limited to armchair-edged GNRs containing exclusively hexagonal rings. Can we synthesize nonplanar GNRs with cove and fjord edges or nonhexagonal rings (pentagonal and heptagonal rings) embedded structures in the solution?

Can we synthesize zigzag-edged GNRs in the liquid phase with ambient stability by rational design of functional substituents at the periphery? The zigzag edge configuration may show localized edge states that can be spin polarized, thus offering GNRs for spintronic applications.

How can we fabricate single GNR-based nanoelectronic or spintronic devices?

How can the dispersibility of GNRs be further improved to satisfy the water-dispersibility for the potential applications in biotechnology and biomedicine?

that are expected to render GNRs with striking magnetic or spintronic properties based on theoretical calculations have remained unexplored in solution syntheses. In addition, heteroatom doping is another effective strategy for modulating the electronic structure of GNRs and may allow localized edge states that can be spin-polarized. Hence, edge engineering and heteroatom doping of GNRs with desirable liquid-phase dispersibility are important challenges to be resolved.

(ii) The scope of introduced side groups or chains must be expanded (e.g., appropriate donor/acceptor groups or functional polymers of various topological architectures such as dendritic polymers), which may not only improve the processability in the liquid phase but also allow the control of the optical/electronic properties of GNRs.

(iii) The achievement of single ribbons in the liquid phase provides great opportunities to control the alignment of single ribbons in their supramolecular nanostructures, such as nanowires or thin films, which enable improved performance of the GNR-based device. For other physical methods, such as magnetic or electrical fields, the alignment of GNRs remains to be explored for the practical device fabrication [60,61]. Moreover, GNRs with ultrahigh molecular weight or lateral length are very important for device fabrications, especially for the achievement of single GNR-based devices. Thus far, AB-type Diels-Alder polymerization renders the synthesis of ultralong (>500 nm) GNRs with tunable width and bandgaps [27]. Nevertheless, other synthetic approaches toward ultrahigh/high molecular weight GNRs in solution remain to be further developed. Therefore, to overcome the above challenges, further breakthroughs in the organic and polymer synthesis of liquid-phase dispersible GNRs are undoubtedly required.

Disclaimer Statement

The authors declare no competing financial interest.

Acknowledgments

This work was financially supported by National Natural Science Foundation of China (21774076 and 51573091), Program of the Shanghai Committee of Science and Technology (17JC1403200 and 19XD1421700), Program of Shanghai Eastern Scholar, European Union's Horizon 2020 research and innovation program under grant agreement No 696656 (Graphene Flagship Core2), the German Research Foundation (DFG) within the Cluster of Excellence 'Center for Advancing Electronics Dresden (cfaed)' and EnhanceNano (No. 391979941), as well as the European Social Fund and the Federal State of Saxony (ESF-Project 'GRAPHD', TU Dresden).

References

1. Han, M.Y. *et al.* (2007) Energy band-gap engineering of graphene nanoribbons. *Phys. Rev. Lett.* 98, 206805
2. Yazyev, O.V. (2013) A guide to the design of electronic properties of graphene nanoribbons. *Acc. Chem. Res.* 46, 2319–2328
3. Datta, S.S. *et al.* (2008) Crystallographic etching of few-layer graphene. *Nano Lett.* 8, 1912–1915
4. Campos-Delgado, J. *et al.* (2008) Bulk production of a new form of sp2 carbon: crystalline graphene nanoribbons. *Nano Lett.* 8, 2773–2778
5. Chen, Z.H. *et al.* (2007) Graphene nano-ribbon electronics. *Phys. E.* 40, 228–232
6. Guo, X. *et al.* (2013) Designing π-conjugated polymers for organic electronics. *Prog. Polym. Sci.* 38, 1832–1908
7. Müllen, K. (2014) Evolution of graphene molecules: structural and functional complexity as driving forces behind nanoscience. *ACS Nano* 8, 6531–6541
8. Chen, L. *et al.* (2012) From nanographene and graphene nanoribbons to graphene sheets: chemical synthesis. *Angew. Chem. Int. Ed.* 51, 7640–7654
9. Narita, A. *et al.* (2015) New advances in nanographene chemistry. *Chem. Soc. Rev.* 44, 6616–6643
10. Jordan, R.S. and Rubin, Y. (2017) The allure of metallic stripes: single-sized narrow ribbons of graphene. *Chem* 2, 11–19
11. Jordan, R.S. *et al.* (2017) Synthesis of N = 8 armchair graphene nanoribbons from four distinct polydiacetylenes. *J. Am. Chem. Soc.* 139, 15878–15890
12. Narita, A. *et al.* (2019) Solution and on-surface synthesis of structurally defined graphene nanoribbons as a new family of semiconductors. *Chem. Sci.* 10, 964–975
13. Li, X. *et al.* (2008) Chemically derived, ultrasmooth graphene nanoribbon semiconductors. *Science* 319, 1229–1232
14. Elías, A.L. *et al.* (2010) Longitudinal cutting of pure and doped carbon nanotubes to form graphitic nanoribbons using metal clusters as nanoscalpels. *Nano Lett.* 10, 366–372
15. Jiao, L. *et al.* (2010) Facile synthesis of high-quality graphene nanoribbons. *Nat. Nanotechnol.* 5, 321–325
16. Sakaguchi, H. *et al.* (2014) Width-controlled sub-nanometer graphene nanoribbon films synthesized by radical-polymerized chemical vapor deposition. *Adv. Mater.* 26, 4134–4138
17. Pan, Z. *et al.* (2011) Wrinkle engineering: a new approach to massive graphene nanoribbon arrays. *J. Am. Chem. Soc.* 133, 17578–17581
18. Narita, A. *et al.* (2015) Bottom-up synthesis of chemically precise graphene nanoribbons. *Chem. Rec.* 15, 295–309
19. Talirz, L. *et al.* (2016) On-surface synthesis of atomically precise graphene nanoribbons. *Adv. Mater.* 28, 6222–6231
20. Cai, J. *et al.* (2010) Atomically precise bottom-up fabrication of graphene nanoribbons. *Nature* 466, 470–473

21. Ruffieux, P. *et al.* (2016) On-surface synthesis of graphene nanoribbons with zigzag edge topology. *Nature* 531, 489–492
22. Liu, J. *et al.* (2015) Toward cove-edged low band gap graphene nanoribbons. *J. Am. Chem. Soc.* 137, 6097–6103
23. Kim, K.T. *et al.* (2013) Charge-transport tuning of solution-processable graphene nanoribbons by substitutional nitrogen doping. *Macromol. Chem. Phys.* 214, 2768
24. Miao, D. *et al.* (2018) Toward thiophene-annulated graphene nanoribbons. *Angew. Chem. Int. Ed.* 130, 3650–3654
25. Li, G. *et al.* (2018) A modular synthetic approach for band-gap engineering of armchair graphene nanoribbons. *Nat. Commun.* 9, 1687
26. Vo, T.H. *et al.* (2014) Bottom-up solution synthesis of narrow nitrogen-doped graphene nanoribbons. *Chem. Commun.* 50, 4172–4174
27. Abbas, A.N. *et al.* (2014) Deposition, characterization, and thin-film-based chemical sensing of ultra-long chemically synthesized graphene nanoribbons. *J. Am. Chem. Soc.* 136, 7555–7558
28. Reuven, D.G. *et al.* (2012) Self-assembly of metallopolymer guided by graphene nanoribbons. *J. Mater. Chem.* 22, 15689–15694
29. Huang, Y. *et al.* (2015) Temperature-dependent multidimensional self-assembly of polyphenylene-based "rod–coil" graft polymers. *J. Am. Chem. Soc.* 137, 11602–11605
30. Huang, Y. *et al.* (2018) Supramolecular nanostructures of structurally defined graphene nanoribbons in the aqueous phase. *Angew. Chem. Int. Ed.* 57, 3366–3371
31. Akhavan, O. *et al.* (2012) Nontoxic concentrations of PEGylated graphene nanoribbons for selective cancer cell imaging and photothermal therapy. *J. Mater. Chem.* 22, 20626–20633
32. Radocea, A. *et al.* (2017) Solution-synthesized chevron graphene nanoribbons exfoliated onto H: Si (100). *Nano Lett.* 17, 170–178
33. Keerthi, A. *et al.* (2017) Edge functionalization of structurally defined graphene nanoribbons for modulating the self-assembled structures. *J. Am. Chem. Soc.* 139, 16454–16457
34. Narita, A. *et al.* (2014) Bottom-up synthesis of liquid-phase-processable graphene nanoribbons with near-infrared absorption. *ACS Nano* 8, 11622–11630
35. Schwierz, F. (2010) Graphene transistors. *Nat. Nanotechnol.* 5, 487–496
36. Xu, Z. and Zheng, Q.S. (2007) Elementary building blocks of graphene-nanoribbon-based electronic devices. *Appl. Phys. Lett.* 90, 223115
37. Costa, P.S. *et al.* (2018) Chevron-based graphene nanoribbon heterojunctions: localized effects of lateral extension and structural defects on electronic properties. *Carbon* 134, 310–315
38. Gemayel, M.E. *et al.* (2014) Graphene nanoribbon blends with P3HT for organic electronics. *Nanoscale* 6, 6301–6314
39. Kim, K.T. *et al.* (2013) Synthesis of graphene nanoribbons with various widths and its application to thin-film transistor. *Carbon* 63, 202–209
40. Schwab, M.G. *et al.* (2012) Structurally defined graphene nanoribbons with high lateral extension. *J. Am. Chem. Soc.* 134, 18169–18172
41. Narita, A. *et al.* (2014) Synthesis of structurally well-defined and liquid-phase-processable graphene nanoribbons. *Nat. Chem.* 6, 126–132
42. Vo, T.H. *et al.* (2014) Large-scale solution synthesis of narrow graphene nanoribbons. *Nat. Commun.* 5, 3189
43. Yang, X. *et al.* (2008) Two-dimensional graphene nanoribbons. *J. Am. Chem. Soc.* 130, 4216–4217
44. Shekhirev, M. and Sinitskii, A. (2017) Solution synthesis of atomically precise graphene nanoribbons. *Phys. Sci. Rev.* 2, 20160108
45. Dossel, L. *et al.* (2011) Graphene nanoribbons by chemists: nanometer-sized, soluble, and defect-free. *Angew. Chem. Int. Ed.* 50, 2540–2543
46. Daigle, M. *et al.* (2017) Helically coiled graphene nanoribbons. *Angew. Chem. Int. Ed.* 129, 6309–6313
47. Yang, W. *et al.* (2016) Bottom-up synthesis of soluble and narrow graphene nanoribbons using alkyne benzannulations. *J. Am. Chem. Soc.* 138, 9137–9144
48. Konnerth, R. *et al.* (2015) Tuning the deposition of molecular graphene nanoribbons by surface functionalization. *Nanoscale* 7, 12807–12811
49. Hu, Y. *et al.* (2018) Bandgap engineering of graphene nanoribbons by control over structural distortion. *J. Am. Chem. Soc.* 140, 7803–7809
50. Slota, M. *et al.* (2018) Magnetic edge states and coherent manipulation of graphene nanoribbons. *Nature* 557, 691–695
51. Schwab, M.G. *et al.* (2015) Bottom-up synthesis of necklace-like graphene nanoribbons. *Chem. Asian J.* 10, 2134–2138
52. Li, G. *et al.* (2016) Efficient bottom-up preparation of graphene nanoribbons by mild Suzuki-Niyaura polymerization of simple triaryl monomers. *Chem. Eur. J.* 22, 9116–9120
53. Shekhirev, M. *et al.* (2017) Interfacial self-assembly of atomically precise graphene nanoribbons into uniform thin films for electronics applications. *ACS Appl. Mater. Interfaces* 9, 693–700
54. Kastler, M. *et al.* (2005) Influence of alkyl substituents on the solution- and surface-organization of hexa-peri-hexabenzocoronenes. *J. Am. Chem. Soc.* 127, 4286–4296
55. Huang, Y. *et al.* (2016) Poly (ethylene oxide) functionalized graphene nanoribbons with excellent solution processability. *J. Am. Chem. Soc.* 138, 10136–10139
56. Huang, Y. *et al.* (2018) Intrinsic properties of single graphene nanoribbons in solution: synthetic and spectroscopic studies. *J. Am. Chem. Soc.* 140, 10416–10420
57. Hill, J.P. *et al.* (2004) Self-assembled hexa-peri-hexabenzocoronene graphitic nanotube. *Science* 304, 1481–1483
58. Yamamoto, Y. *et al.* (2006) Photoconductive coaxial nanotubes of molecularly connected electron donor and acceptor layers. *Science* 314, 1761–1764
59. Watson, M.D. *et al.* (2001) Big is beautiful–"aromaticity" revisited from the viewpoint of macromolecular and supramolecular benzene chemistry. *Chem. Rev.* 101, 1267–1300
60. Craats, A.M. *et al.* (1999) Record charge carrier mobility in a room-temperature discotic liquid-crystalline derivative of hexabenzocoronene. *Adv. Mater.* 11, 1469–1472
61. Craats, A.M. *et al.* (2003) Meso-epitaxial solution-growth of self-organizing discotic liquid-crystalline semiconductors. *Adv. Mater.* 15, 495–499
62. Ivanov, I. *et al.* (2017) Role of edge engineering in photoconductivity of graphene nanoribbons. *J. Am. Chem. Soc.* 139, 7982–7988
63. Llinas, J.P. *et al.* (2017) Short-channel field-effect transistors with 9-atom and 13-atom wide graphene nanoribbons. *Nat. Commun.* 8, 633
64. Candini, A. *et al.* (2017) High photoresponsivity in graphene nanoribbon field-effect transistor devices contacted with graphene electrodes. *J. Phys. Chem. C* 121, 10620–10625
65. Zschieschang, U. *et al.* (2015) Electrical characteristics of field-effect transistors based on chemically synthesized graphene nanoribbons. *Adv. Electron. Mater.* 1, 1400010